Enhanced photocatalytic activity of the hierarchical structure TiO_2 hollow spheres with reactive (001) facets for the removal of toxic heavy metal Cr(VI)

Yong Yang,[a] Guozhong Wang,*[a] Quan Deng,[a] Huiming Wang,[a] Yunxia Zhang,[a] Dickon H.L. Ng[b] and Huijun Zhao[a,c]

Supporting information

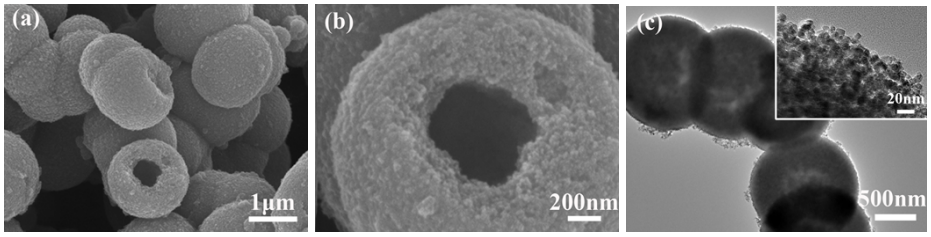

Figure S1. (a) and (b) FESEM images of SF-THS, and (c) TEM image of SF-THS, inset is the enlarged TEM image of the sphere surface edge.

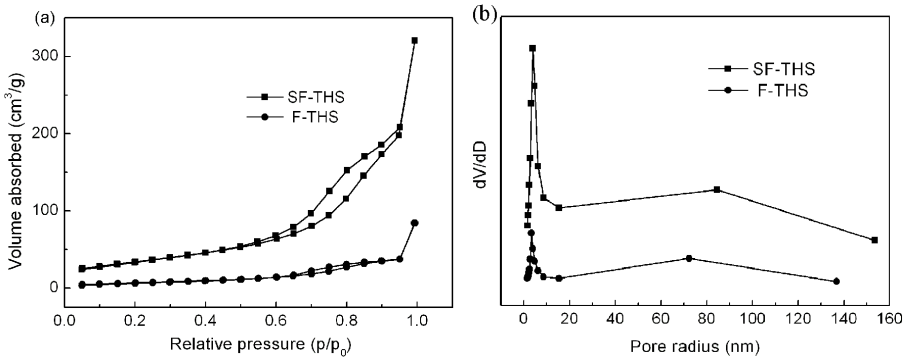

Figure S2. (a) Nitrogen sorption isotherms and (b) pore size distribution curves of the different samples.

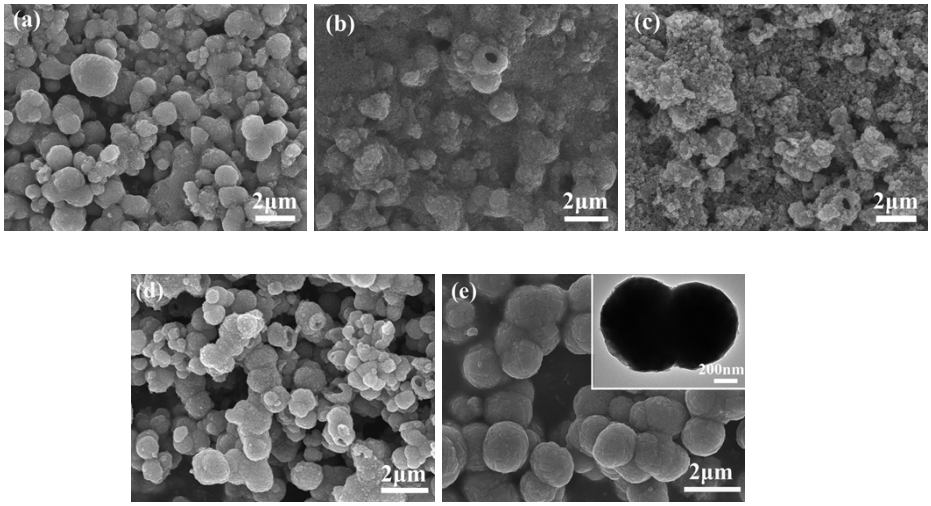

Figure S3. FESEM images of the products prepared at 180 °C for 10 h with the different RF: (a) 0; (b) 0.5; (c) 1; (d) 2; (e) 5 (the inset shows the TEM image).

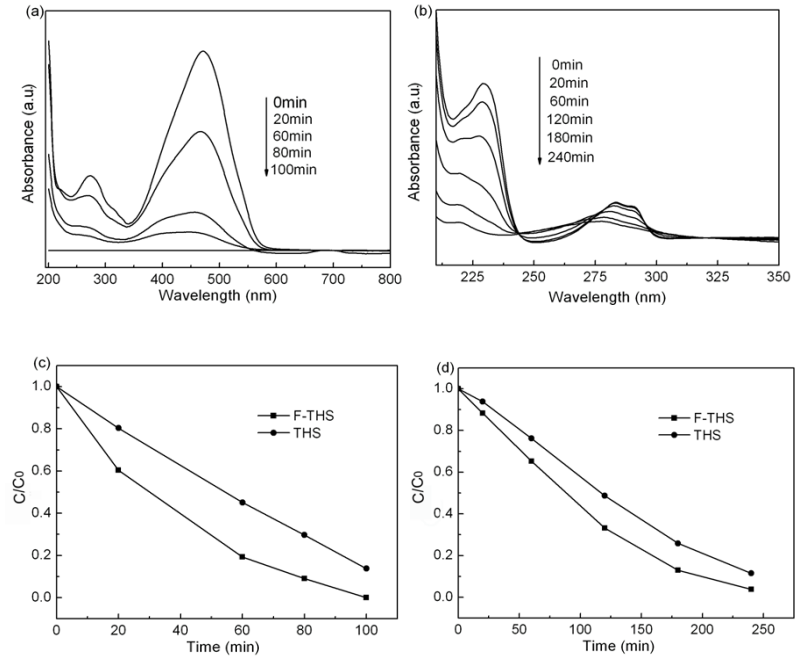

Figure S4. Time-dependent optical absorbance spectra for the (a) methyl orange and (b) 2,4-dichlorophenoxyacetic acid solution in the presence of F-THS. (c) methyl orange and (d) 2,4-dichlorophenoxyacetic acid normalization concentrations versus the exposure time to UV light with the different TiO_2 catalysts. C_0 is the starting concentration, C is concentration of the remaining methyl orange or 2,4-dichlorophenoxyacetic acid at time t.

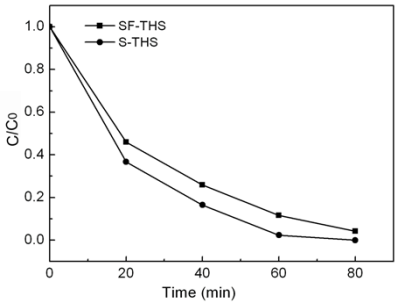

Figure S5. The photocatalytic removal of Cr(VI) with the different catalysts.

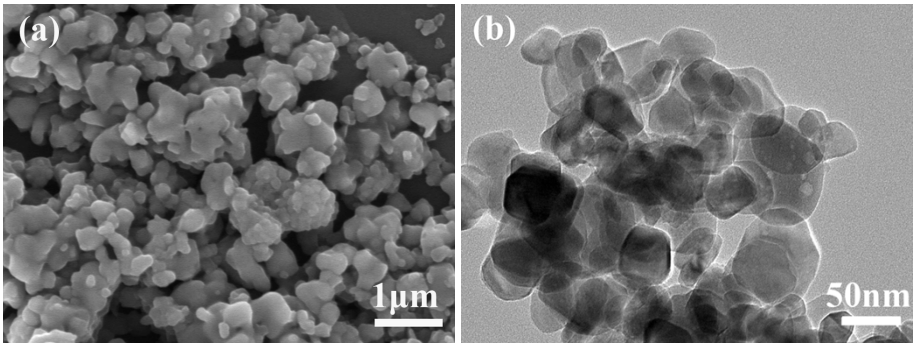

Figure S6. (a) FESEM image of the micron-sized TiO_2 and (b) TEM image of the nanometer-sized TiO_2.

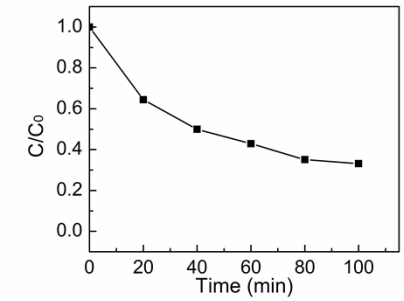

Figure S7. The photocatalytic removal of Cr(VI) with Degussa P25 as the photocatalyst, C_0 is the initial concentration of Cr(VI) (10 mg/L), catalyst loading: 0.5 g/L, pH value: 4.

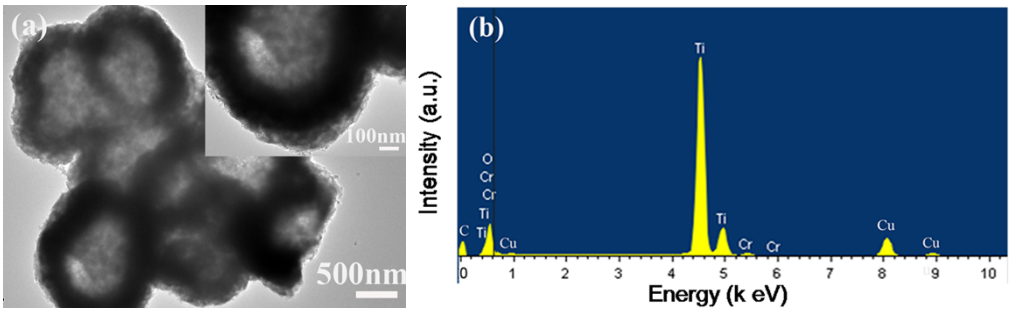

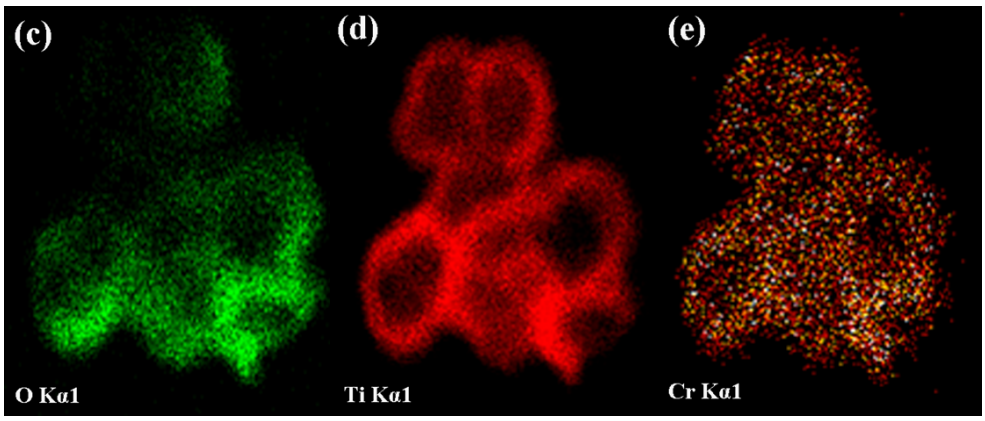

Figure S8. (a) TEM image (inset is the high magnification image) and (b) EDX pattern of THS after photocatalytic reaction. Element mapping of O, Ti and Cr taken from (a) are presented in (c), (d) and (e) at O $K_{\alpha1}$ edge (525 eV), Ti $K_{\alpha1}$ edge (4527 eV) and Cr $K_{\alpha1}$ (5412 eV), respectively.

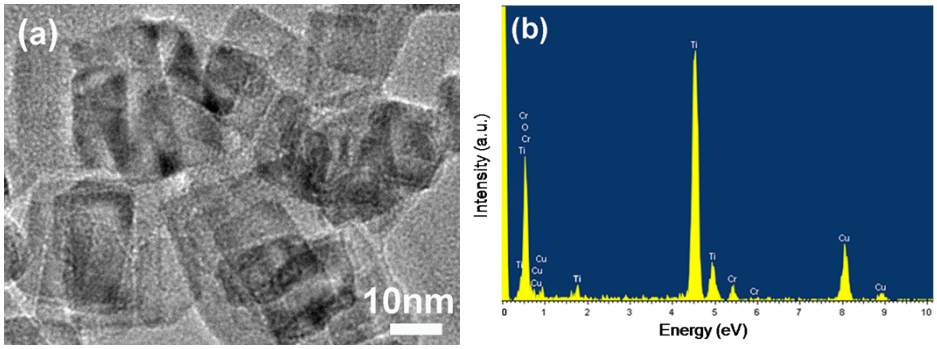

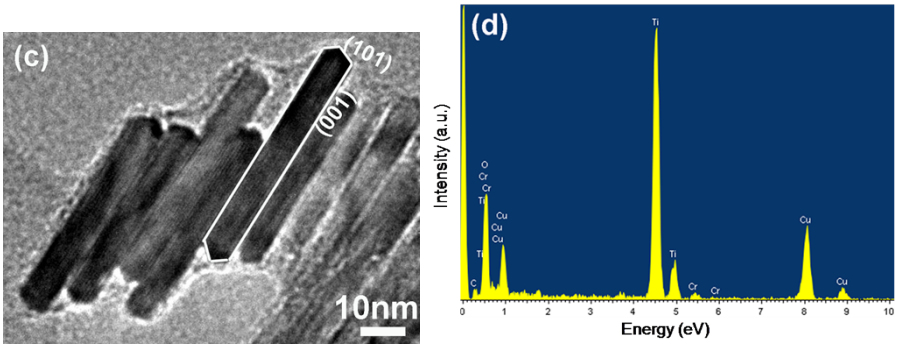

Figure S9. TEM images and EDX patterns of the reactive (001) facets exposed nanosheets after photocatalytic treatment of Cr(VI) recorded from (a), (b): [001] and (c), (d): [100] direction.

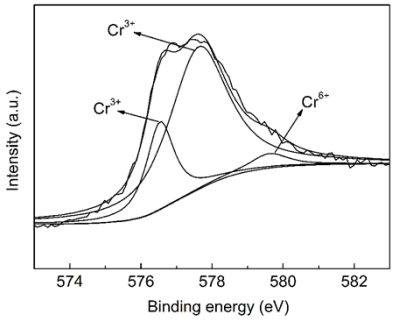

Figure S10. The $Cr2p^{3/2}$ high-resolution XPS spectrum of THS powder after photocatalytic reaction.

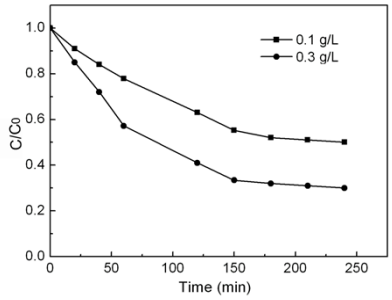

Figure S11. The photocatalytic removal of Cr(VI) with the different amount of photocatalyst THS.